View metadata, citation and similar papers at core.ac.uk

brought to you by CORE

provided by IntechOpen

We are IntechOpen, the world's leading publisher of Open Access books Built by scientists, for scientists

4,800
Open access books available

122,000
International authors and editors

135M
Downloads

Our authors are among the

154
Countries delivered to

TOP 1%
most cited scientists

12.2%
Contributors from top 500 universities

CLARIVATE ANALYTICS BOOK CITATION INDEX INDEXED

WEB OF SCIENCE™

Selection of our books indexed in the Book Citation Index in Web of Science™ Core Collection (BKCI)

Interested in publishing with us?
Contact book.department@intechopen.com

Numbers displayed above are based on latest data collected.
For more information visit www.intechopen.com

18

Complementary Use of NMR to X-Ray Crystallography for the Analysis of Protein Morphological Change in Solution

Shin-ichi Tate, Aiko Imada and Noriaki Hiroguchi
Department of Mathematical and Life Sciences, Hiroshima University
Japan

1. Introduction

A vast amount of protein structure data is going to pave new ways in protein structure research. They improved the quality of predicted protein structure from its primary sequence (Sanchez and Sali 2000). The possible protein interaction sites to small ligand and/or the other proteins could be predicted based on the protein complex structures in the Protein Data Bank (PDB) (Morris et al. 2009). The combined use of bioinformatics with the protein structure data has been frequently giving invaluable outcomes to facilitate the understanding on the experimental results in biochemistry and molecular biology. *In silico* protein structure analyses are now already essential approaches in protein research.

Protein structural data, most of which came from X-ray crystallography, are also useful to expand the protein structure analysis in solution, when combined with NMR. NMR chemical shift perturbation of a protein caused by the interaction with a compound, for example, allows sensitive identification of the interaction sites on protein (Shuker et al. 1996). This NMR derived binding site information with the protein structure facilitates drug design (Hajduk et al. 1997). This chemical shift-based approach is also applied to the protein-protein interaction, which enables to build a model protein complex structure (de Vries, van Dijk and Bonvin 2010, Dominguez, Boelens and Bonvin 2003). Although these approaches are now prevailingly used, there are limitations in their application. The approaches assume that the target protein retains the X-ray structure in solution and also negates the possible structural change caused by binding to a compound or a partner protein. Some of the proteins are known to have different domain arrangement from those in crystal (Skrynnikov et al. 2000a); it is often the case for the protein having domains linked by flexible linker. In addition, it is commonly found that proteins show structural change in response to compound binding or interaction with the other protein (Evenas et al. 2001). To expand the utility of protein structure data in the PDB in solution protein science, we need new NMR techniques to overcome the known limitations in the existing approaches, which could determine the structure changed from the one by X-ray in binding to a ligand or a partner protein to improve the modelled complex structure, for example.

Protein structure change caused by interaction with other molecules is primarily important in discussing protein functional regulation. The structural change is not limited in the region around the binding site. Sometimes, it also causes rather global change including domain

rearrangement or subunit rearrangement. Hereafter, we would mention to this global structural change as '*protein morphological change*' to emphasize its large amplitude in motion.
Protein morphological change is characterized by the considerable difference in the spatial arrangement of structural units from their original positions; structural units may include domain, subunit, or, sometimes, a small segment comprising of secondary structures. In the case, each unit mostly retains the original structure, except for the limited region engaged in the interaction (Fig. 1). The high-resolution unit structures from X-ray are therefore used as the templates in analyzing the morphological changes, for example, to see how the domains are rearranged upon ligand binding. As exemplified by Luciferase morphological change upon ligand binding, each domain shows little structural change, except for the intrinsically flexible loops (Nakatsu et al. 2006, Conti, Franks and Brick 1996) (Fig. 1). The bound form structure can be reconstituted from the apo-structure by rotating the small domain relative to the other (Fig. 1).

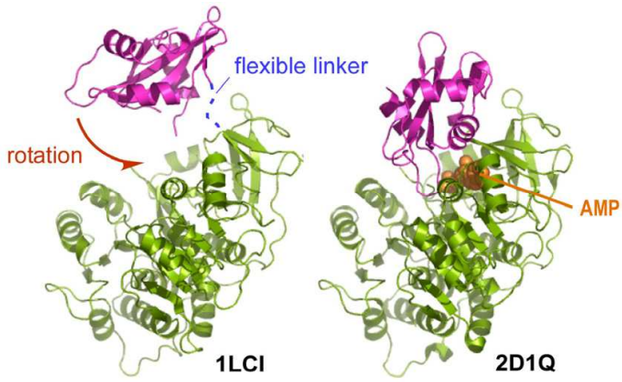

Fig. 1. Protein morphological change. Domain rearrangement of Luciferase upon binding to ATP. PDB codes 1LCI and 2D1Q for apo- and AMP-bound forms. Small domain is rotated over onto the large domain upon ligand binding. Both domains basically retain the structures in apo-form only with slight local changes.

The conventional NMR structure determination relying on NOEs and vicinal spin couplings, both of which give the only short-range structural information, does not properly determine the domain arrangement, particularly in the case that domains are connected by a linker and there are little inter-domain contacts. The accumulation of the less quantitative short-range structural information may even result in the erroneous determination of domain arrangement. It requires the global structural information that directly defines the domain arrangement.
In addition to the requirement for the global structural information, the molecular size limitation in solution NMR spectroscopy is another obstacle to work on the protein morphology by NMR. The conventional NMR approach has severe size limitation in determining protein structure, which is practically 30 kDa. Proteins having multiple domains tend to be greater than 50 kDa, thus the conventional NMR approach is not usable in protein morphology analysis.
Protein morphological change is of the great significance in biology, but there has not been any appropriate NMR techniques for this purpose, so far. With this concern, we have devised a new NMR approach, DIORITE (Determination of the Induced ORIentation by Trosy Experiments), that can overcome the obstacles in the conventional approaches, lacking global structural information and size limitation (Tate 2008, Tate, Shimahara and

Utsunomiya-Tate 2004). In this chapter, we are going to describe this NMR method from its theoretical backgrounds to applications to demonstrate how it works on the protein morphology analyses. This gives a complementary view on protein structure in solution, which is not seen by X-ray crystallography, although it requires high-resolution crystal structure as a template for the analysis. The combined use of high-resolution X-ray structure and its morphology analysis in solution by DIORITE may expand our understanding how protein works more vividly.

2. Residual anisotropic spin interactions

Conventional NMR structure analysis based on the short-range spin interactions does not give any global structural information required in protein morphology study. The residual anisotropic spin interactions, which become apparent for a '*weakly*' aligned protein, give molecular orientation information relative to the magnetic field. And the information gives the clues to analyze protein morphology.

Two different types of residual anisotropic spin interactions are observed in the amide ^{1}H-^{15}N spin pair on a peptide plane; one is the nuclear spin dipolar-dipolar interaction and the other is anisotropic shielding effect against the external magnetic field, which is called as chemical shift anisotropy (CSA) (Fig. 2).

These anisotropic spin interactions are not observed on a NMR spectrum for protein in an isotropic solution, where protein rapidly tumbles. Because of the rapid rotation that allows for protein to direct the entire angles against a magnetic field, anisotropic spin interactions are completely canceled for isotropic sample. In contrast, protein dissolved in a magnetically ordering liquid crystalline medium, for example, experiences some rotational restrictions by steric bump with the liquid crystalline molecules. Thus, it leads to incomplete cancellation of anisotropic spin interactions, which should give the residual anisotropic spin interactions observed on a spectrum. In a properly tuned liquid crystalline concentration, there is enough space to allow protein tumbling to some extent. The protein in an aligned liquid crystalline medium, accordingly, still can give high resolution NMR signals. In the higher liquid crystalline concentration, the protein tumbling becomes substantially limited and its NMR signals become severely broadened to prohibit their spectral observation. The condition that protein tumbling is slightly restricted to achieve incomplete cancellation of the anisotropic spin interactions, but it still gives narrow lines enough for the observation on a NMR spectrum is called as a '*weak*' alignment (Bax 2003).

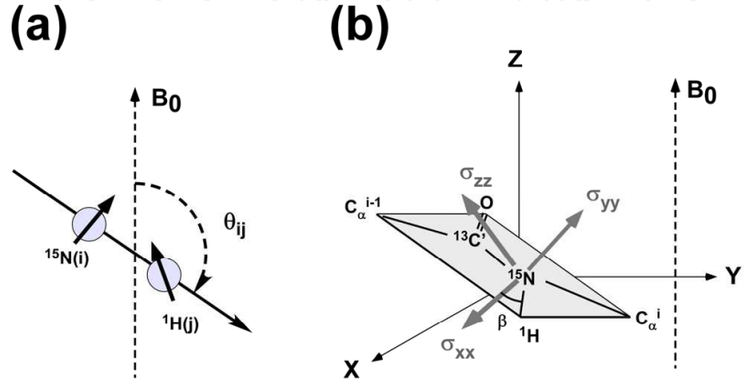

Fig. 2. Two anisotropic spin interactions observed for amide ^{1}H-^{15}N spin pair. (a) dipolar interaction. (b) ^{15}N chemical shift anisotropy (CSA) effect.

The spin interactions apparent only under a weakly aligning condition are the residuals by incomplete cancellation of the spatially anisotropic spin interactions. The effects are, therefore, called as '*residual*' anisotropic spin interactions. In the following text, we will focus on two types of the residual anisotropic spin interactions on a peptide plane prior to describe the DIORITE; they are the residual dipolar coupling (RDC) and the residual CSA (RCSA). DIORITE relies on these two anisotropic spin interactions, and their theoretical basics will be helpful in understanding DIORITE approach.

2.1 Residual dipolar coupling, RDC

Residual nuclear spin dipolar interaction (RDC) gives the direction of the internuclear vector against the magnetic field. In the peptide bond of a protein labeled with ^{15}N, the RDC for amide ^{15}N nucleus defines the angle between the NH bond vector and a magnetic field (Fig. 2a).

The RDCs amide ^{1}H-^{15}N spin pairs are the measurement of common choice, primarily due to the good spectral dispersion of the ^{1}H-^{15}N correlation signals on a 2D spectrum. The RDCs are obtained from a pair of ^{1}H-^{15}N HSQC spectra measured without ^{1}H decoupling during t_1 evolution period of ^{15}N spin; one spectrum is for the isotropic sample, and the other is for the aligned (Fig. 3). On a ^{1}H-coupled ^{1}H-^{15}N HSQC spectrum, each peak gives a pair of signals split along the ^{15}N axis (Fig. 3). The split width of signal for the isotropic sample corresponds to single-bond spin coupling ($^{1}J_{NH}$) between the covalently bonded ^{1}H and ^{15}N nuclei, around 93 Hz (Fig. 3a). Split width for the aligned sample gives the value deviated from $^{1}J_{NH}$ (Fig. 3b). The difference in the apparent $^{1}J_{NH}$ values between the isotropic and aligned sample is the RDC. In this section, we will describe how the RDCs can define the alignment tensor of protein, by describing its theoretical background.

2.2 Theoretical description on RDC

We focus on the amide ^{1}H-^{15}N spin pair here; i and j represent ^{1}H and ^{15}N nucleus, respectively. The dipolar Hamiltonian to describe the magnitude of dipolar split is written in the following equation in a laboratory frame under the high-field limit condition:

$$H_{ij}{}^{D}(t) = -\left(\frac{\mu_0}{4\pi}\right)\frac{\gamma_i\gamma_j h}{2\pi^2 r_{ij}{}^3} I_{iz}I_{jz}P_2(\cos\Theta(t)) \quad (1)$$

where r_{ij} is the distance between ^{1}H and ^{15}N atoms, γ_i and γ_j are the gyromagnetic ratios for ^{1}H and ^{15}N nuclear spins, respectively. As physical constants, h is Planck constant and μ_0 is vacuum permeability. I_{iz} and S_{jz} represent the spin angular-momentum operators for ^{1}H and ^{15}N spins, respectively. The angular part of the dipolar Hamiltonian is described by the second rank Legendre function, $P_2(\cos\Theta(t))$, here $\Theta(t)$ is a time-dependent angle between the magnetic field and the internuclear vector (NH bond vector in the present context) (Fig. 4a). In determining molecular orientation by RDC, bond libration effect is negligible due to its faster motion relative to molecular tumbling; bond libration occurs in a few hundred psec time regimes, whilst molecular tumbling happens in nsec range. In this sense, r_{ij} is defined as time-averaged effective internuclear distance, thus it is estimated to be slightly longer (1.04 Å) than the static bond length (1.02 Å).

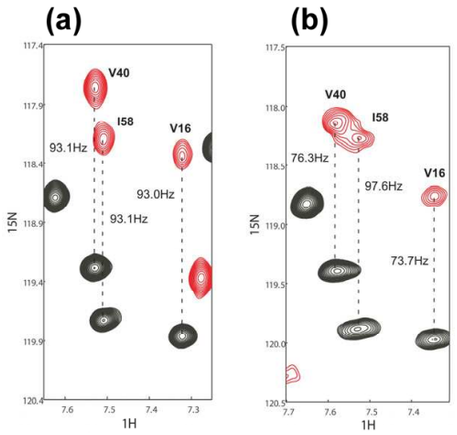

Fig. 3. RDC measurement with ^{1}H coupled HSQC. Isotropic sample (a) and aligned sample (b). Split with for each paired signals corresponds to $^1J_{NH}$. The apparent $^1J_{NH}$ is changed for aligned sample. The change in $^1J_{NH}$ from the isotropic value is RDC.

The experimentally measured residual dipolar couplings, D_{ij}^{res}, is represented as the time-averaged expectation value for the dipolar Hamiltonian, Eq. (1).

$$D_{ij}^{res}(t) = -\left(\frac{\mu_0}{4\pi}\right)\frac{\gamma_i\gamma_j h}{2\pi^2 r_{ij}^3} < P_2(\cos\Theta(t)) > \tag{2}$$

The angle brackets denote the time-averaged resultant. The molecule in an isotropic tumbling gives no RDC, $< P_2(\cos\Theta(t)) >= 0$, due to the isotropic distribution of molecular orientation. On the other hand, the molecule in an anisotropic tumbling incompletely vanishes the term, $< P_2(\cos\Theta(t)) >\neq 0$. The magnitudes of the residual values are related to the molecular orientation angle and the alignment order against a magnetic field. The theoretical description to relate the RDCs to the orientation angles and orders will be given below.

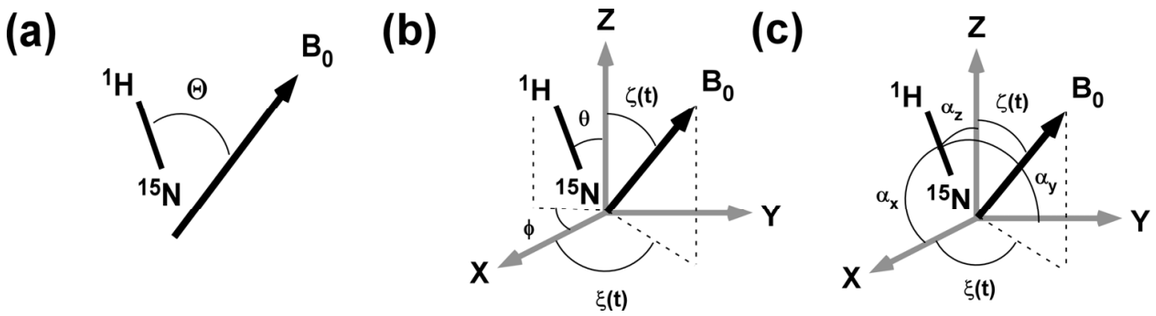

Fig. 4. Three different representations for NH bond vector against a magnetic field. (a) Angle dependency of the ^{1}H-^{15}N RDC is described by Θ , the angle between the NH bond vector and a magnetic field. (b) NH bond vector on a molecular coordinate system, whose direction is defined by polar angles (θ,ϕ). Molecular reorientation relative to a magnetic field is described by the time dependent polar angles ($\xi(t),\zeta(t)$). (c) NH bond vector is recast by direction cosines to three molecular axes.

Protein structure is represented by the atom positions in a Cartesian coordinate system. This coordinate system is referred as the molecular coordinate system here. The orientation of each NH bond vector in a protein is described by polar angles (θ, ϕ) in the molecular coordinate system (Fig. 4b). Now, we neglect the local NH bond libration, thus, the angles θ and ϕ are time-independent. Likewise, at any instant in time, the orientation of the magnetic field is described by the time dependent polar angles, ($\xi(t),\zeta(t)$) (Fig. 4b). The molecule reorients against a magnetic field in a time dependent manner; this molecular motion is represented by the directional change of the magnetic field on the molecular coordinate system (Fig. 4b). The polar angles defining a magnetic field direction, therefore, are described as time dependent parameters.
The Legendre function $P_2(\cos\Theta(t))$ is expanded by the spherical harmonics according to the spherical harmonic addition theorem:

$$P_2(\cos\theta(t)) = \tfrac{4\pi}{5}\sum_{q=-2}^{2} Y^*{}_{2q}(\theta,\varphi)Y_{2q}(\zeta(t),\xi(t)) \tag{3}$$

where the Y_{2q}'s are the normalized spherical harmonics. Using Eq. (3), the residual dipolar coupling (Eq. (2)) is expressed with spherical harmonics:

$$D_{ij}{}^{res} = -\left(\tfrac{\mu_0}{4\pi}\right)\tfrac{\gamma_i\gamma_j h}{2\pi^2 r_{ij}{}^3}\tfrac{4\pi}{5}\sum_{q=-2}^{2} Y^*{}_{2q}(\theta,\varphi)\left\langle Y_{2q}(\zeta(t),\xi(t))\right\rangle \tag{4}$$

In Eq. (4), the five time-averaged spherical harmonics $\left\langle Y_{2q}(\zeta(t),\xi(t))\right\rangle$ with q = -2, -1, 0, 1, 2 defines the molecular alignment angles and its magnitudes. Recasting these five terms makes more intuitively acceptable representation to describe the molecular alignment state, which is Saupe's order matrix.
The use of Saupe's order matrix reforms Eq. (4).

$$D_{ij}{}^{res} = -\left(\tfrac{\mu_0}{4\pi}\right)\tfrac{\gamma_i\gamma_j h}{2\pi^2 r_{ij}{}^3}\tfrac{4\pi}{5}\sum_{k,l=x,y,z} S_{kl}\cos(\alpha_k)\cos(\alpha_l) \tag{5}$$

where, S_{kl} is an element in Saupe's order matrix. The Saupe order matrix is a traceless, symmetric, 3 × 3 matrix, thus it comprises of five independent elements. In the representation using Saupe's order matrix, each bond vector orientation is defined by direction cosines against the molecular coordinate axes (Fig. 4c). The Saupe's order matrix elements that are made of the time-averaged spherical harmonics $\left\langle Y_{2q}(\zeta(t),\xi(t))\right\rangle$ are shown below:

$$\begin{aligned}
S_{xz} &= \sqrt{\tfrac{3}{8}}\sqrt{\tfrac{4\pi}{5}}\left(\left\langle Y_{21}(\xi(t),\zeta(t))\right\rangle - \left\langle Y_{2-1}(\xi(t),\zeta(t))\right\rangle\right)\\
S_{yz} &= i\sqrt{\tfrac{3}{8}}\sqrt{\tfrac{4\pi}{5}}\left(\left\langle Y_{21}(\xi(t),\zeta(t))\right\rangle + \left\langle Y_{2-1}(\xi(t),\zeta(t))\right\rangle\right)\\
S_{xy} &= i\sqrt{\tfrac{3}{8}}\sqrt{\tfrac{4\pi}{5}}\left(\left\langle Y_{22}(\xi(t),\zeta(t))\right\rangle - \left\langle Y_{2-2}(\xi(t),\zeta(t))\right\rangle\right)\\
S_{xx} - S_{yy} &= \sqrt{\tfrac{3}{2}}\sqrt{\tfrac{4\pi}{5}}\left(\left\langle Y_{22}(\xi(t),\zeta(t))\right\rangle + \left\langle Y_{2-2}(\xi(t),\zeta(t))\right\rangle\right)\\
S_{zz} &= \sqrt{\tfrac{4\pi}{5}}\left\langle Y_{20}(\xi(t),\zeta(t))\right\rangle
\end{aligned} \tag{6}$$

The Saupe order matrix describes the angle and the order for aligned protein relative to the magnetic field. Diagonalization of the Saupe order matrix gives the alignment tensor; its principal values represent the alignment order along each principal axis and the principal axes define the direction of the aligned molecule. In the alignment tensor, z-axis is defined as the most ordered axis. An asymmetry, $\eta = (S_{xx} - S_{yy}) / S_{zz}$, represents the deviation from axially symmetric ordering. The orientation of the alignment tensor axes (principal axes) is described on the molecular coordinate system by Euler angles.

In the alignment tensor axes system (the alignment tensor frame), the residual dipolar coupling D_{ij}^{res} is represented by the following two parameters, A_a and A_r, that include two non-zero average spherical harmonics:

$$\begin{aligned} \left\langle Y_{20}(\xi(t),\zeta(t)) \right\rangle &= \sqrt{\tfrac{5}{4\pi}} S_{zz} = \sqrt{\tfrac{5}{4\pi}} A_a \\ \left\langle Y_{2\pm2}(\xi(t),\zeta(t)) \right\rangle &= \sqrt{\tfrac{5}{24\pi}} \left(S_{xx} - S_{yy} \right) = \sqrt{\tfrac{15}{32\pi}} A_r \end{aligned} \tag{7}$$

Using the parameters, the D_{ij}^{res} is re-represented in a more intuitive form:

$$D_{ij}^{res} = -\left(\tfrac{\mu_0}{4\pi}\right) \tfrac{\gamma_i \gamma_j h}{2\pi^2 r_{ij}^3} \left[A_a (3\cos^2\theta' - 1) + \tfrac{2}{3} A_r \sin^2\theta' \cos 2\varphi' \right] \tag{8}$$

where the polar angles (θ', ϕ') define the orientation of NH bond vector in the alignment tensor frame. A_a and A_r represent the axial and rhombic components of the order magnitudes, respectively. The orientation of protein relative to a magnetic field is defined by the Euler angles (α, β, γ) that describes the position of the alignment tensor frame on the molecular coordinate system.

2.3 Residual chemical shift anisotropy, RCSA

Another anisotropic spin interaction associated with the amide ^{15}N nucleus comes from chemical shift anisotropy, CSA (Fig. 2b). This effect is observed as ^{15}N chemical shift change induced by a weak alignment (Fig. 5). The alignment induced chemical shift change is called as residual CSA, RCSA (Kurita et al. 2003).

The chemical shift for each nucleus is related to the shielding against the magnetic field by the electrons surrounding the nucleus, which is called as chemical shielding. In general, the spatial distribution of electrons around the nucleus is not uniform but rather spatially anisotropic. Therefore, the chemical shielding effect to the nucleus should change according to the orientation molecule against a magnetic field; the chemical shift for the nucleus can be orientation dependent. However, the molecule in an isotropic solution averages the orientation dependent shielding effects by its rapid isotropic tumbling, thus giving the orientation independent '*isotropic chemical shifts*' on a spectrum.

As in the case of the dipolar interaction, a weak alignment makes the orientation dependency of CSA observable, due to the incomplete averaging of anisotropic shielding effects. The amide ^{15}N has significantly large CSA, because of the substantial anisotropic distribution of the electron on a peptide plane. Protein in a weakly aligned state, thus, shows significant chemical shift changes along ^{15}N axis relative to its isotropic positions (Fig. 5). Although it is not described in detail in this manuscript, carbonyl ^{13}C has also large CSA and it shows significant RCSA under a weakly aligning state (Lundstrom, Hansen and Kay 2008).

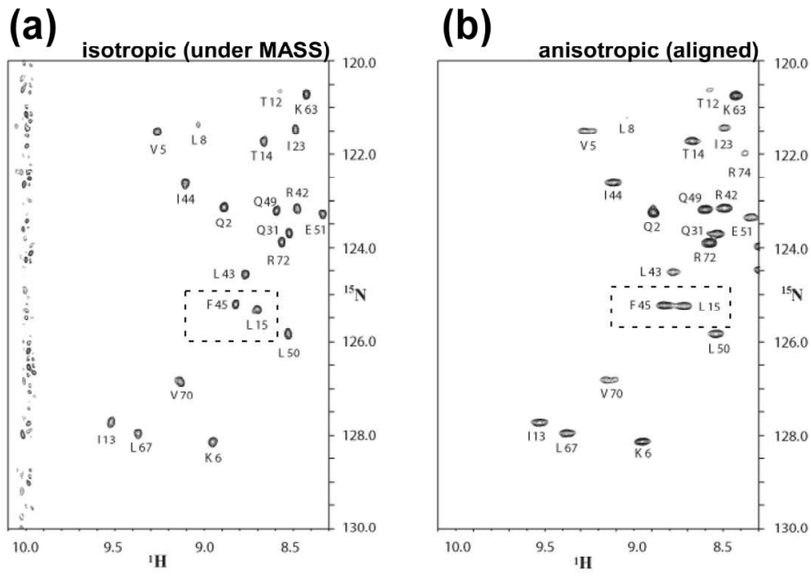

Fig. 5. ^{15}N chemical shift change induced by a weak alignment. ^{1}H-^{15}N HSQC spectra are compared for ^{15}N labeled ubiquitin dissolved in 7.5% (w/v) DMPC/DHPC/CTAB ternary bicelle solution between isotropic and aligned states: (a) under the magic angle sample spinning condition, giving an isotropic spectrum, (b) the aligned condition. Chemical shift changes along the ^{15}N axis caused by a weak alignment are clearly observed, for examples the signals in dotted square. These spectral changes come from the incomplete cancellation of ^{15}N chemical shift anisotropy (CSA) effect under a weak aligning condition. The change along the ^{15}N axis is the value for the residual CSA, RCSA.

The alignment induced chemical shift change, or RCSA, $\Delta\delta$, is expressed with Sauce's order matrix, S_{ij} , as for the RDC, Eq. (5). Based on this relation, we can also determine the alignment tensor of the molecule as done with the RDC.

$$\Delta\delta = \tfrac{2}{3} \sum_{i=x,y,z} \sum_{j=x,y,z} \sum_{k=x,y,z} S_{ij} \cos(\theta_{ik}) \cos(\theta_{jk}) \delta_{kk} \tag{8}$$

Here, $\cos\theta_{ij}$ denotes the direction cosine between *i*-axis in the molecular coordinate system and *j*-axis in the CSA tensor principal axis. The principal value for the CSA tensor axis *k* is represented by δ_{kk} . The spatially anisotropic distribution of the electrons around a nucleus is represented by a tensor (CSA tensor), where each principal axis represents the shielding magnitude. The ^{15}N CSA tensor axes are drawn on a peptide plane (Fig. 2b).

The alignment tensor is determined based on the Saupe order matrix obtained through the relation in Eq. (8) for a set of $\Delta\delta$ data. It is noted that in calculating the Saupe order matrix, we require the knowledge of the CSA tensor that is defined by the relative orientation of the CSA tensor frame on a peptide plane and the magnitudes of the principal values. In the case of the RDC, we assumed the effective interatomic distance, r_{ij}, to a fixed value. In contrast to the RDC based analysis that requires one pre-defined value for r_{ij}, the RCSA analysis requires five pre-defined parameters; two principal values δ_{zz}, δ_{xx} , with $\delta_{xx} + \delta_{yy} + \delta_{zz} = 0$, and Euler angles (α, β, γ) that define the CSA tensor orientation on a peptide plane. The RCSA based alignment tensor determination is therefore, much more knowledge demanding.

The ^{15}N CSA tensor is known to be significantly dependent on the local structure, particularly backbone torsion angle (Yao et al. 2010). Experimentally determined ^{15}N CSA tensors are reported with a various method (Fushman, Tjandra and Cowburn 1999, Cornilescu and Bax 2000, Boyd and Redfield 1999, Hiyama et al. 1988, Kurita et al. 2003). These data give consensus ^{15}N CSA tensor values for the residue in each type of secondary structure, α-helix, β-sheet and others. Practically, the use of the secondary structure specific ^{15}N CSA tensor values can determine the alignment tensor within experimental errors.
Experimental determination of ^{15}N CSA tensor for protein in solution is possible using the weak alignment technique. We previously proposed the method using magic-angle sample spinning to determine the accurate secondary structure specific ^{15}N CSA tensor, in which the bicellar media was used for a weak alignment (Kurita et al. 2003). In this experiment, we used only one aligned state, thus, only determined the ^{15}N CSA tensors in a secondary structure specific manner.
Recently, Bax and co-workers have applied this approach to determine the residue specific ^{15}N CSA tensors for a protein, where they used five more different aligning states to solve the Saupe order matrix for each residue (Yao et al. 2010). The residue specific ^{15}N CSA tensor determination that requires multiple aligned states of protein is rather demanding experiments, which require a various loop mutant to change aligning angle (Yao et al. 2010). However, the continuous effort to collect the residue specific ^{15}N CSA tensors in the similar way by Bax and co-workers will establish a clearer correlation between the ^{15}N CSA tensor and backbone torsion angles and also local interactions like hydrogen bonding, which may allow the prediction of the appropriate ^{15}N CSA tensor values from the structure. The refined ^{15}N CSA tensors will further improve the quality of alignment tensor analysis with the RCSA, although the present RCSA based approach gives an acceptable result.

3. Achieving weak alignment

In applying the residual anisotropic spin interactions described above, it is required to make a protein in a weakly aligned state. The aligning protein has to be carefully tuned to make the anisotropic interactions observable in a spectrum with keeping the spectral resolution and intensity. Alignment order is practically tuned to approximately 10^{-3}, giving about 20 Hz in maximum absolute magnitude for amide ^{1}H-^{15}N RDC. To achieve a weak alignment, some artificial medium has to be used, because the inherent magnetic susceptibility of a globular protein is too small to align to the desired extent, except for some heme-containing proteins having substantial magnetic susceptibility associated with a heme group. In this section, we will review some media for weak alignment.

3.1 Magnetically aligning liquid crystalline media

Magnetically ordering liquid crystalline media are commonly used. Discoidal phospholipid assembly, bicelle, is one of the prevailingly used materials for a weak alignment of protein (Ottiger and Bax 1999, Ottiger, Delaglio and Bax 1998, Tjandra and Bax 1997).. The bicelle is composed of a mixer of dimyristoylphosphatidylcholin (DMPC) and dihexynoyl-phosphatidylcholine (DHPC) in a ratio of 3:1. This phospholipid binary mixture forms lipid bilayers disks 30 nm – 40 nm in diameter. Bicelle has substantial magnetic susceptibility, and it spontaneously aligns under magnetic field with the normal of the bicelle surface staying perpendicular to the magnetic field (Fig. 6a).
In the experiments to measure the anisotropic spin interactions, an appropriate amount of bicelle is put into protein solution. In a high magnetic field, bicelles align and the aligned

discoidal liquid crystalline molecules limit the space for protein tumbling. Bicelle has flat surface, thus, the protein involved in the aligned bicellar media will be surrounded by flat walls. Because of the steric clash, protein does not rotate freely near the bicelle wall, which will hider some orientations of the protein. This hindrance on some orientations for the protein in the bicellar medium causes incomplete rotational averaging of the anisotropic interactions, which thus makes the residual anisotropic interactions observables (Berlin, O'Leary and Fushman 2009, Vijayan and Zweckstetter 2005, Zweckstetter 2008).

The aligning magnitude is readily tuned by the bicelle concentration; higher bicelle concentration induces the stronger order of alignment. The bicelle made of the binary phospholipid mixture involving DMPC and DHPC has neutral charge on its surface. Therefore, most proteins do not stick to bicelles. Protein aligns through collisional interaction described above.

Surface charge doping to the bicellar surface is possible. Incorporation of CTAB, cetyl trimethyl ammonium bromide, to DMPC/DHPC binary phospholipid bicelle generates the positively charged surface, while the addition of SDS, sodium dodecyl sulphate, makes it negatively charged. The surface charge doping to bicelle changes the aligning property from that by neutral bicelle. In charged bicellar solutoin, electrostatic interactions between the medium and protein become apparent. This makes it sometimes difficult to use the charged bicelle to acidic or basic proteins such as nucleic acid binding proteins.

There are some limitations in the bicelle application as aligning media. One is in the limited temperature range to keep bicelle in a liquid crystalline phase; it is typically 27°C – 45°C. Some proteins precipitate in this temperature range, and the bicelle is not used for such proteins. In addition, the bicelle is only stable around neutral pH; in acidic or basic solution, the bicellar medium tends to make phase-separation and loses aligning ability. To avoid the limitations associated with the physicochemical properties of the bicelle medium, other liquid crystalline media have been reported. By properly selecting the medium, we can now achieve weak alignment for rather various types of proteins, each of which requires its own optimal temperature, pH, and ionic strength (Prestegard, Bougault and Kishore 2004).

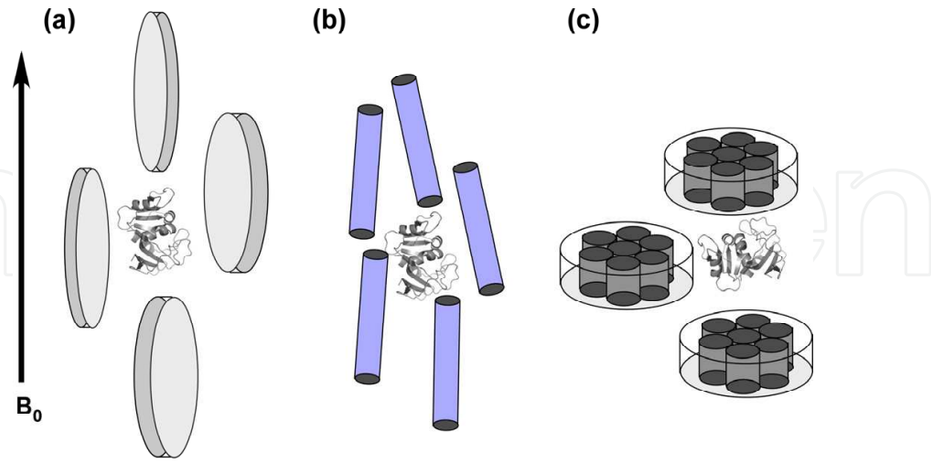

Fig. 6. Weak alignment made by using various media. (a) Discoidal shape phospholipid bicelle medium, (b) rod-like filamentous phage and (c) Purple membrane. Because of significant anisotropic magnetic susceptibility, the molecules spontaneously align in a magnetic field. Proteins within the aligning media are aligned through the collisional interaction or electrostatic interactions with the aligning molecules.

3.2 Naturally occurring materials that spontaneously align in a magnetic field

Some naturally available molecules that spontaneously align in a magnetic field are also used for weak alignment. Purple membrane is one example, which forms two-dimensional crystal lattice structure of bacteriorhodopsin (bR) that is rich in α-helices (Fig. 6b). Purple membrane constitutes of ordered α-helices and thus it has intrinsic high anisotropic magnetic susceptibility. Because of the structural characteristics, purple membrane can spontaneously align in a high magnetic field.

Suspension of purple membrane is added into protein solution to achieve a weak protein alignment. The alignment magnitude is tuned by the purple membrane concentration in a sample solution, as was the case for the bicelle medium (Sass et al. 1999). Purple membrane is the discoidal protein lipid complex, and it aligns with its normal parallel to the magnetic field. Purple membrane is rich in negative charge on its surface. Therefore, protein is aligned through the electrostatic interaction not collisional interaction.

Filamentous phage, which is made of a rod-like coat protein, is another example of the naturally occurring molecule used for weak alignment. Because of the highly anisotropic shape of the filamentous phage, it spontaneously aligns in a high magnetic field, with its rod axis parallel to a magnetic field (Fig. 6c). Filamentous phage has also negatively charged surface, thus it induces protein alignment through electrostatic interactions with protein as in the case of purple membrane. The alignment order can be tuned by adjusting the concentration of the phage suspension in protein solution.

The use of purple membrane and filamentous phage cannot be applied to basic proteins that are positively charged. The basic proteins tightly adsorb onto the negatively charged surfaces of the aligning molecules through the electrostatic interaction, which result in extreme ordering of proteins and thus prohibit observing high resolution NMR signals.

3.3 Compressed acryl amide gel

The other method uses anisotropically compressed acrylamide gel (Tycko, Blanco and Ishii 2000, Ishii, Markus and Tycko 2001, Sass et al. 1999). Acrylamide hydrogel has cavities to capture proteins within, whose cavity size is changed by altering the ratios of the composing chemicals, acrylamide and bis-acrylamide. Acrylamide forms a linear polymer chain and bis-acrylamide makes bridge to link acrylamide liner polymers, thus, the increased ratio of bis-acrylamide generates smaller cavity.

The acrylamide gel has a spatially isotropic cavity. Protein in the gel does not show any preferential orientation, and thus it shows no residual anisotropic spin interaction on its NMR spectrum. Protein alignment by the gel is achieved by inducing the spatial anisotropy to the cavities in the gel.

In a weakly alignment experiment using the gel, a cast gel including a protein solution is inserted into a NMR sample tube. There are two ways to make anisotropically compressed gel; one is to press the gel along the NMR tube (compressed gel) and the other is squeeze it in the lateral dimension, thus it becomes stretched vertically (stretched gel) (Fig. 7).

In vertical compression, gel is cast to have a shorter diameter than the inner diameter for NMR sample tube. After inserting the gel, vertically compressed with glass rod in the tube (Fig. 7a). On the other hand, stretched gel is made from the cast gel having a slightly larger diameter than that the inner diameter of the tube; the gel is inserted into the tube by using tapered device (Chou et al. 2001) (Fig. 7b). Because of the different pressing direction, these two preparations change the protein orientation to each other.

The charge doping in the anisotropically compressed gel is also possible. Negative charge is doped by replacing a part of acrylamide with acrylate, while a positive charge is introduced by adding DADMAC, diallyldimethylammonium chloride, in casting gel chip. These charge doping changes aligning property, because electrostatic interaction between protein and the gel becomes active.

Acrylamide gel is neutral and thus it induces protein alignment through collisional interaction between protein and walls having spatial anisotropy made by the compression. The non-charged acrylamide gel is readily used for any types of protein, independent on its pKa value. On the other hand, the charged gel is sometimes troublesome in achieving weak alignment of basic or acidic proteins, due to their adsorption onto the gel.

The aligning order magnitude is also tuned by changing the concentration of acrylamide and/or the ratio of the composing chemicals and also the diameter of the cased gel chip. In addition, the extent of the charge doping may have to be considered in some cases. There are more parameters to adjust than that for the liquid crystalline media. We, therefore, need some trial experiments to gain the optimal gel condition to have the anisotropic spin interactions observable in enough spectral resolution.

The great advantage in using the compressed gel is in the chemical stability of acrylamide gel. In using acrylamide gel for a weak alignment, we do not worry about the sample conditions including temperature, salt concentration, and solution pH. Under any sample conditions, we can align protein by the compressed gel. It is a keen difference from the limitation in applying liquid crystalline media and also in using the naturally occurring materials. The compressed gel is used as a universal media for weakly aligning protein.

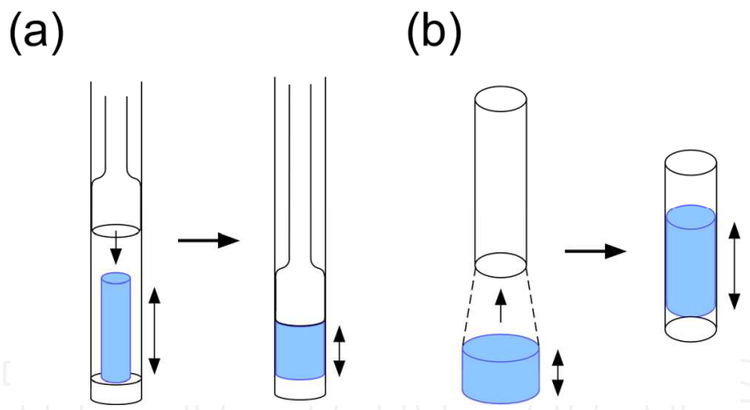

Fig. 7. Anisotropically compressed gels to achieve weak alignment. (a) Vertically compressed gel. (b) Laterally compressed, thus, stretched gel. Cast gel chip (blue) is inserted into a NMR glass tube. In the vertical compression, the cast gel is pressed by a glass rod in NMR tube. These compressions induce spatially anisotropic cavities within the acrylamide gel.

3.4 Protein structure in aligned media – Is it natural?

A weak alignment of protein is prerequisite for the analysis of protein morphology by NMR, because it relies on the anisotropic spin interactions that happen only under a weak aligned condition. Because protein is dissolved in an artificial medium like magnetically ordering liquid crystalline solution, one should worry about the structure under the condition; the domain orientation in such a medium represents the real state of the protein in an isotropic solution?

The mechanisms for aligning protein in magnetically aligned bicelle solution and rod-like filamentous phage suspension are well understood. The observed RDCs can be reproduced with using the protein crystal structure by the simulation based on the mechanism. The successful reproduction of the RDCs for the protein aligned by bicelle or filamentous phage supports that the proposed theory properly describes the state of protein in the aligning media.
According to the theory, the observed residual anisotropic spin interactions can be established by a small fraction of protein experiencing the rotational restriction through the collision between the protein and the aligning molecule. In using the charged filamentous phage, the electrostatic interactions are also active in inducing the rotational restriction on the protein near the medium. The fraction for that is around 0.1% of the total number of protein molecules in the sample. The interactions have to be weak and transient. The inter-molecule interactions, therefore, do not actively align the protein but just prohibit some fraction of the protein orientation near the medium. Under the condition, the aligning media do not induce artificial protein conformation or domain arrangement, because the prohibited orientation angles neat the medium is solely determined by the intrinsic molecular shape of protein in the bulk solution.
The structural perturbation by the medium is easily monitored by the NMR spectral changes. If the medium tightly interacts with protein to change the structure, some of the chemical shifts should change from those found in an isotropic state.
The bicellar medium is in the liquid crystalline state over its phase-transition temperature. Under the temperature, it becomes a micelle solution that does not align in a magnetic field, thus does not induce protein alignment. If protein in this micelle solution does not show apparent spectral changes from the solution, including no micelle, we exclude the possibility that the bicelle induces a structural change to the protein.
In the case of the charged filamentous phage, the increased concentration of cations, which shield the surface charge on the medium, impairs the ordering of the media in a magnetic field. The magnitudes of the anisotropic spin interactions for the protein in the phage suspension, therefore, are proportion to the cation concentration. If the spectral changes show linear dependency on the cation concentration, we could rule out the structural changes caused by the interaction with the medium.
Using compressed acrylamide gel allows the direct spectral comparison between the samples in the reference gel (non-compressed gel) and the isotropic solution without gel to see if any structure change happens through the interaction with the gel.
In general, under weakly aligning conditions, the spectral changes caused by the interaction with the media are rather small, ensuring that no apparent structural changes happen to protein in the media, even in the cases of multiple-domain proteins.

4. RDC-based domain orientation analysis – Basics and limitation

In this section, we will describe the experimental procedure to determine the domain orientation of a multiple-domain protein, from the RDC data collection to structure determination. In addition, the limitations in the RDC based analysis will be discussed to emphasize the necessity of our TROSY based DIORITE approach that follows.

4.1 Collecting the RDC data

RDC is measured on a pair of ^{1}H coupled HSQC spectra for the samples in isotropic and anisotropic states. The ^{1}H coupled HSQC spectrum gives a pair of split peaks along ^{15}N axis

for each ^{1}H-^{15}N correlation. The doubled number of peaks on a ^{1}H coupled HSQC spectrum may increase signal overlaps that obstacle the accurate reading of peak positions. To avoid this drawback, a particular NMR technique is used to separate the up- and down-field components into different 2D spectra, IPAP-HSQC. IPAP-HSQC gives two separate spectra that have in-phase and anti-phase doubles, respectively. Addition or subtraction of the spectra will give two separate 2D spectra displaying only up-field or down-filed components of each doublet. This signal separation reduces signal overlap on a ^{1}H coupled HSQC spectrum, and keeps the spectral resolution to the same extent as in the original HSQC spectrum (Fig. 3).

The separation width between the up- and down-field components measured from IPAP-HSQC spectra gives $^{1}J_{NH}$ for isotropic sample and $^{1}J_{NH} + D_{NH}^{res}$ for aligned sample. Therefore, the RDC, D_{NH}^{res}, is obtained by their difference.

4.2 Domain orientation analysis based on the RDC data

Here, we describe the domain orientation analysis based on the RDCs. The domain orientation analysis should be done for the protein whose structure is already known by X-ray. The primal interest of the analysis is in exploring the domain reorientation upon interaction with the other protein or ligand. In the cases, each domain is assumed to retain the same structure as in crystal.

As described in the theory section, the alignment tensor for a weakly aligned protein is determined based by the RDCs and its structure coordinate, Eq. (5). In Eq. (5), direction cosines are calculated from the structure coordinate. Because the Saupe order matrix consists of five independent elements, we need more than five RDC data to determine the Saupe order matrix for the corresponding part. The singular value decomposition (SVD) to the matrix comprising of the relations for the observed RDCs will give the Saupe order matrix (Losonczi et al. 1999). Diagonalizing the Saupe order matrix gives the alignment tensor frame orientation relative to the molecular coordinate system and the magnate of the orders along each principal axis. As described in the theory part, the alignment tensor frame orientation is defined by the Euler angles (α, β, γ).

We consider a two-domain protein here. And we assume that the high resolution structure of each domain is available, and each domain structure is the same as in the crystal. Based on the collected RDCs, the alignment tensor for each domain is independently determined according to the above procedure. As schematically drawn in Fig. 8, the determined tensor frames for each domain are used as a guide to define solution domain orientation; one domain coordinate is rotated to make an overlay its tensor frame onto the other (Fig. 8). It is noted here, the RDCs do not provide any distance information between the domains. If the inter-domain segment has high flexibility, the additional distance restraints may be required to build the entire structure, which should come from the other experiments like paramagnetic relaxation enhancement (Clore and Schwieters 2002).

Alignment tensor determined by the RDCs has four possible orientations. Inversion around each principal axis gives the same RDCs values. Therefore, the inversion is not discriminated experimentally. To alleviate this ambiguity in orientation angle, additional alignment states using different aligning media, including charged bicelle, or charged acrylamide gel, will be used. In domain orientation analysis, however, the structural restrictions, which include the length of the inter-domain linker or possible inter-domain steric clash, may allow to define one inter-domain orientation even using a single aligning experiment.

The alignment tensor magnitudes along each principal axis represent the extent of the aligning order. If they differ between the domains, which may indicate that each rotates differently to each other. The aligning orders give the insight into the domain dynamics in a protein.

4.3 Significance of the domain orientation analysis by RDCs

The domain orientation analysis for protein in solution gives an invaluable outcome, even its high-resolution structure is available. There are some cases to show the different domain arrangements between solution and crystalline structures. The RDC analysis on maltose binding protein (MBP) in the complex with β-cyclodextrin has shown that the relative domain orientation in solution was different from that in the crystal (Skrynnikov et al. 2000b). This may indicate the crystal contact causes a subtle change in domain orientation. Bacteriophage T4 lysozyme in solution was shown to have a more open conformation relative to the crystal structure, which was also analyzed by the RDCs (Goto et al. 2001). This observation appears compatible with steric requirements for the ligand bindings.

These examples illustrate how the RDC based domain analysis complements X-ray crystallography in determining the relative domain orientation or protein morphology. The complementary role of the RDC based analysis is considerably emphasized in exploring the domain rearrangement upon binding to the other protein or ligand. Even if the complex structure cannot be solved by X-ray, the complex structure is determined by the RDCs in a solution state when the structure in a ligand-free form is available. This approach does not require tedious and time-consuming NOE analysis as required in conventional NMR structure determination, but just needs the backbone resonance assignments and a set of IPAP-HSQC spectra. The structure determination is, therefore, much more efficient over the conventional NMR structure determination.

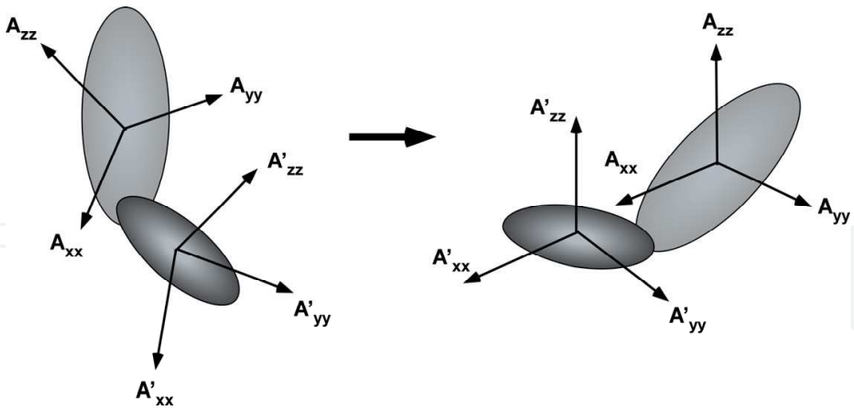

Fig. 8. Schematic representation for the procedure to determine the relative domain orientation based on the alignment tensors for each domain. Sets of RDC data determine the alignment tensor for each domain, independently. The domain orientation of a protein is established by rotating one domain coordinate to make an overlay of its tensor frame on the other.

4.4 Molecular size limitation in the RDC based approach

The domain orientation analysis with the RDCs is now recognized as a useful technique to elucidate overall protein morphology in solution, complementing the X-ray structure

analysis. This approach has, however, severe size limitation. Here, this obstacle in the RDC application is discussed.

The size limitation comes from the rapid transverse relaxation rate of one of the split components observed on a 2D IPAP-HSQC spectrum. The high-filed component shows faster transverse relaxation rate than that of the other. This component has even faster relaxation rate than that of HSQC counterpart. This is due to cross-correlated relaxation interference to amide ^{15}N spin relaxation process; for the high-field component, the cross-correlated relaxation process additively affects, while for the low-field component, the interference reduces its relaxation rate. The transverse relaxation process of the HSQC signal is free from the interference.

In measuring the RDCs with IPAP-HSQC for high molecular weight protein, the high-field components of each amide spin pairs will broaden and severely reduce the signal intensities, thus, they will not be observed. In particular, the difficulty in observing the high-field component will be enhanced in an aligned state, due to the appearance of the residual dipolar interactions as relaxation causes. For proteins over 20 kDa, it is usually hard to observe the high-field component in an aligned state, thus making the RDC measurement impossible. The RDC based domain orientation analysis with IPAP-HSQC is practically limited up to around 20 kDa.

Simulation of the line broadening on each component of a double according to molecular size is shown in Fig. 9. In this figure, the low-field component that shows a longer transverse relaxation time and the other having a shorter transverse relaxation time are named as TROSY and anti-TROSY, respectively. The slower transverse relaxation associated with the low-field component is due to the mechanism used in TROSY (Transverse Relaxation Optimized SpetroscopY). As demonstrated on the simulation, the anti-TROSY component shows severe broadening even for the medium-size protein, 20 kDa.

The difference in line widths between the TROSY and anti-TROSY components will become considerable for higher molecular weight proteins. As seen in the simulation, protein over 150 kDa gives severely broadened anti-TROSY signal, which already hard to observe. Protein with 800 kDa never gives observable anti-TROSY signal. The size limitation in the RDC based approach is clearly demonstrated in this simulation.

It should be noted, the TROSY component can retain observable signal intensity even for 800 kDa protein (Fig. 9). This motivated us to devise an approach to determine an alignment tensor only using TROSY components.

4.5 Existing remedy for overcoming the size limitation in the RDC-based approach

Some remedies are proposed to overcome the size limitation the RDC application. They all rely on the TROSY.

The difference in the transverse relaxation rates between the TROSY (low-field) and anti-TROSY (high-field) components split along the ^{15}N axis are explained by the relaxation interference. The same effect is active in the split signals along ^{1}H dimension. In observing the ^{1}H-^{15}N single bond correlation spectrum without decoupling during t_1 and also t_2 durations, each spin pair gives a quartet on a spectrum; split signals in both ^{1}H and ^{15}N dimensions. The pure TROSY signal is the one having the longest transverse relaxation time among the quartets. In using the protein labeled with ^{15}N and ^{2}H, where an unwanted relaxation process is diminished by breaking the ^{1}H-^{1}H dipolar interaction network in a protein, TROSY effect is enhanced, and it allows ^{1}H-^{15}N correlation spectrum for proteins over 100 kDa (Pervushin et al. 1997).

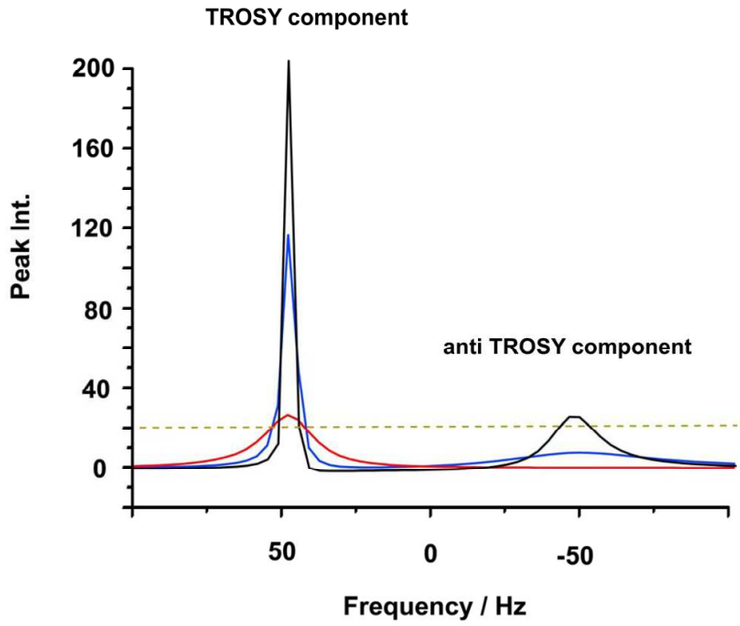

Fig. 9. Simulation of the molecular size dependency of the TROSY and anti-TROSY components observed on a IPAP-HSQC spectrum. The data represent a slice peak along the ^{15}N axis. This simulation assumed a 750 MHz experiment. Black, blue, and red lines are the simulated peaks for the sizes 20 kDa, 150 kDa, and 800 kDa, respectively. The dotted line is assumed the expected noise level.

One proposed remedy is the combinatorial use of TROSY and HSQC. The difference between TROSY and HSQC signals along the ^{15}N axis corresponds to a half of RDC. As discussed above, the transverse relaxation rate of the HSQC signal is slower than that for the anti-TROSY component in a IPAP-HSQC spectra. Therefore, the size limitation problem should be alleviated by replacing anti-TROSY signal with HSQC counterpart. For a 81.4 kDa protein, the transverse relaxation times for the TROSY, anti-TROSY, and HSQC signals are reported to be 65 msec, 10 msec, and 30 msec, respectively (Tugarinov and Kay 2003). In considering the difference between the transverse relaxation times between TROSY and HSQC signals, the combinatorial use does not fully solve the problem, but just alleviates it.
Another remedy is the use of J-scaled TROSY, which is also referred to as J-enhanced (JE) TROSY (Kontaxis, Clore and Bax 2000, Bhattacharya, Revington and Zuiderweg 2010). In this experiment, short J-evolution step is added in the standard TROSY, which induces J-dependent shift change from the standard TROSY shift. In the standard TROSY experiment, the shift difference between the signals along the ^{15}N axis on the same ^{1}H chemical shift corresponds to $^{1}J_{NH}$, whilst in the J-scaled TROSY, this shift difference is changed according to the additional duration for J-evolution. From the magnitude of the shift change induced by the applied J-evolution period, the apparent $^{1}J_{NH}$ coupling value is estimated. If the J-evolution period is applied to allow full recovery of $^{1}J_{NH}$ coupling, the observed signal position should be coincident with that of the HSQC signal. Usually, to gain the signal intensity for the observed signal on J-scaled TROSY, rather limited evolution time is set. In this J-evolution step, the coherences for TROSY and anti-TROSY are mixed; the equivalent

mixing of the two gives the coherence for observed as HSQC signal. The more increased the contribution of the anti-TROSY coherence to the observed signal leads to more broadened signals observed. Therefore, in the J-scaled TROSY experiment, partial recovery of the J-modulation is used to maintain the signal intensities on the J-scaled TROSY spectrum in the observable level.

Signals observed on a J-scaled TROSY spectrum have longer transverse relaxation times than those of the signals on a HSQC spectrum. Their transverse relaxation times, however, are still shorter than those for real TROSY counterparts. The combined use of TROSY and J-scaled TROSY is indeed advantageous over the TROSY/HSQC combination. In determining more accurate RDCs, J-scaled TROSY requires more extent of the mixing of the anti-TROSY coherences, which will result in the lesser sensitive J-scaled TROSY signals. The use of J-scaled TROSY is not the complete remedy for the problem we concern.

In spite of the limitations in the existing approaches, they expanded the RDC application up to 50 kDa protein (Jain, Noble and Prestegard 2003). However, it is also reported that the rapid transverse relaxation of the non-TROSY component is already an obstacle in measuring the RDCs for 81.4 kDa protein . The further expansion of the application limit is expected, and our DIORITE is one of the possible methods used for this purpose.

5. Alignment tensor determination using only TROSY

As discussed above, the molecular size limitation problem in the RDC based domain orientation analysis is not completely overcome, although the existing approaches have given some successful results. Most of the biologically interesting multi domain proteins tend to be over 100 kDa. The existing approaches are not thought to be applied to such higher molecular weight protein. This is because they do not take fully advantages of TROSY spectroscopy, which allows the longest transverse relaxation time for the observed signals. In contrast to the existing approaches, our approach, DIOIRTE, uses only TROSY spectra, where the signals having the longest transverse relaxation times are used. This may give considerable advantages over the existing methods in respect to the size limitation problem. In this section, we will describe the theoretical aspects of the TROSY based alignment tensor determination, which will allow the domain orientation analysis for higher molecular weight proteins ever.

5.1 Alignment induced TROSY shift changes

TROSY shift is changed when protein is transferred from isotropic to anisotropic states. This TROSY shift change along the ^{15}N axis contains the effects of two anisotropic spin interaction observed on a peptide plane; ^{1}H-^{15}N dipolar interaction and ^{15}N CSA. As depicted in Fig. 10, this alignment induced TROSY shift change, $\Delta\delta_{TROSY}$, contains a half of RDC and the full RCSA effects. In a Cartesian representation using the Saupe order matrix, the following relation should fold:

$$\begin{aligned}\Delta\delta_{TROSY} &= -\tfrac{1}{2}\left(\frac{\mu_0}{4\pi}\right)\frac{\gamma_i\gamma_j h}{2\pi^2 r_{ij}{}^3}\frac{4\pi}{5}\sum_{kl=x,y,z} S_{kl}\cos(\alpha_k)\cos(\alpha_l) \\ &+\tfrac{2}{3}\sum_{kl=x,y,z}\sum_{j=x,y,z} S_{kl}\cos(\theta_{kj})\cos(\theta_{lj})\delta_{jj} \\ &= \sum_{kl} S_{lk}\{\tfrac{1}{2}D^0{}_{NH}\cos(\alpha_k)\cos(\alpha_l)+\tfrac{2}{3}\Delta_{kl}\}\end{aligned} \tag{9}$$

$$\Delta_{kl} = \sum_{k,l=x,y,z} \sum_{j=x,y,z} S_{kl} \cos(\theta_{kj}) \cos(\theta_{lj}) \delta_{jj} \tag{10}$$

where, $\cos(\alpha_k)$ is the direction cosine for the NH bond vector relative the molecular axis *k*, *k* = x, y, z. D^0_{NH} is the static dipolar coupling constant, which equals 23.0 and 21.7 kHz for assumed NH bond length 1.02 Å and 1.04 Å, respectively; in solution, the effective NH bond length is estimated to be 1.04 Å, which values includes the bond libration effects. The tem $\cos(\theta_{kj})$ is the direction cosine of the CSA principal axis *j* relative to the molecular axis *k*. The principal value of the CSA tensor along *j* axis is denoted as δ_{jj} . As done for the RDC, the SVD calculation to the equations Eq. (9) for the residues in a protein gives the Saupe order matrix. At least, five $\Delta\delta_{TROSY}$ data are required to determine the Saupe order matrix constituted by five independent elements. The alignment tensor is obtained through the diagonalization of the Saupe matrix.

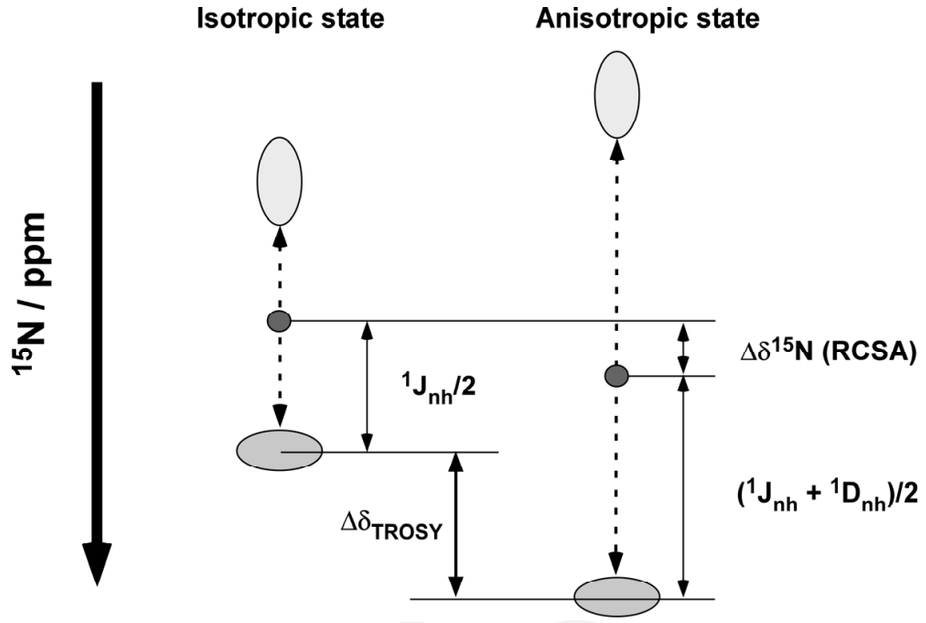

Fig. 10. Schematic drawing of the relationship among the signals for ^{1}H-^{15}N doublet in a ^{1}H coupled HSQC spectra observed for protein in isotropic and aligned states. $\Delta\delta_{TROSY}$ contains the contributions from a half of RDC and full RCSA.

DIORITE is the algorism to determine the alignment tensor solely from TRSOY spectra. It may be expected that DIORITE gives a more accurate alignment tensor over the ^{1}H-^{15}N RDCs, in particular, the case for huge protein over 50 kDa, due to the longest transverse relaxation time of the TROSY signal. DIORITE determines the alignment tensor based on two anisotropic spin interactions; RDC and RCSA. As described in theory part, RCSA contains the tensorial orientational information of the peptide plane against a magnetic field, while RDC gives only the bond vector orientation. RDC value does not change if the peptide plane is rotated along the NH bond axis, although RCSA should significantly change. Because of the inclusion of RCSA effect, DIORITE can discriminate the difference in the peptide plane orientation. Therefore, DIORITE should be more informative over the RDC based analysis in determining the domain orientation of a protein.

5.2 CSA tensor parameters used in DIOIRTE

DIORITE based alignment tensor determination requires ^{15}N CSA tensor for each residue. As discussed in the part for the RCSA, it is not trivial to get accurate ^{15}N CSA tensor for each residue in a protein, because it has significant local structure dependency; backbone torsion angle, hydrogen bonding, and so forth. In the DIORITE analysis, ^{15}N CSA tensors for every residue have to be known as input values.

In the domain orientation analysis with DIORITE, we use a high resolution domain coordinate from X-ray. Therefore, we know the detailed structure on each domain before the analysis. Some recent reports on the experimental determination of the residue specific ^{15}N CSA tensor for small proteins in solution had demonstrated that the ^{15}N CSA tensor value is primarily dependent on the backbone torsion angle. According to this correlation, we proposed the practical protocol for the DIORITE analysis that uses the secondary structure specific ^{15}N CSA tensors as inputs.

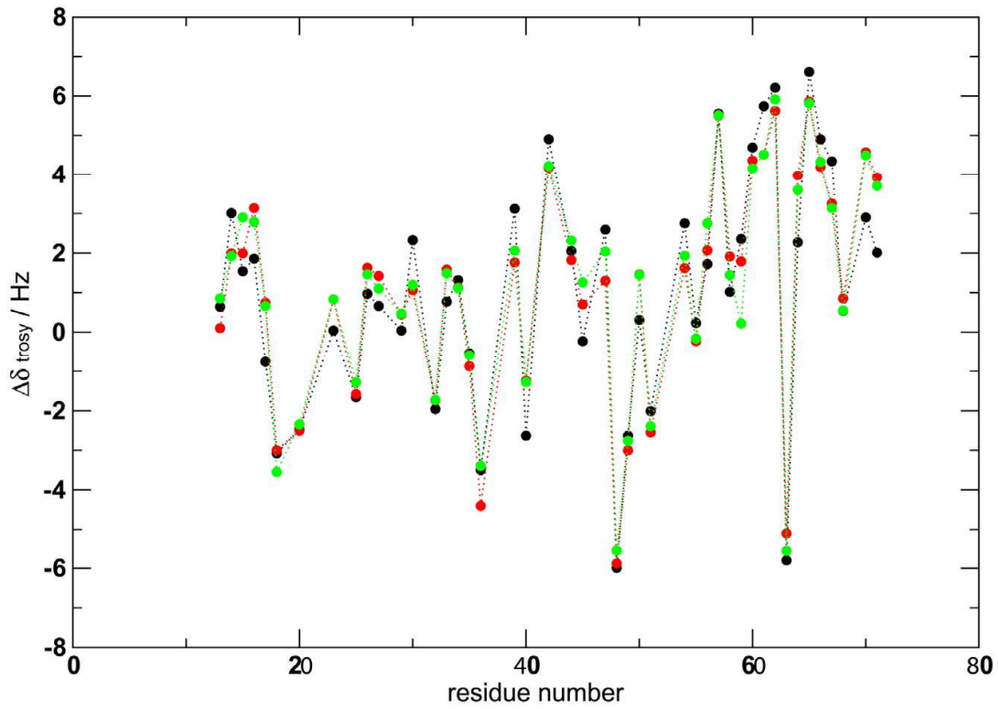

Fig. 11. Comparison of the back-calculated $\Delta\delta_{TROSY}$ obtained by DIORITE algorism using the secondary structure specific and the residue specific ^{15}N CSA tensors. Red and green circles are the values with secondary structure specific and residues specific tensors, respectively. Black circles are the observed $\Delta\delta_{TROSY}$.

The quality of the back calculated $\Delta\delta_{TROSY}$ values were assessed on ubiquitin. The values with the secondary structure specific ^{15}N CSA tensors and those with the residue specific tensors were compared (Fig. 11); the residue specific ^{15}N CSAs used here were determined by a set of elaborate spin relaxation analyses by Bodenhausen and co-workers (Loth, Pelupessy and Bodenhausen 2005). As demonstrated in the comparison, the use of the secondary structure specific ^{15}N CSA tensor gives consistent results with those with residue-

specific values within an error range (Fig. 11). The DIORITE analysis using the secondary structure specific ^{15}N CSA tensors, therefore, can be a practical approach for exploring the domain orientation in a protein.

5.3 DIORITE analysis using different magnetic field strengths

TROSY effect reduces line width along ^{15}N dimension at a higher magnetic field; the original paper on TROSY has estimated the optimal frequency for obtaining the narrowest lines is around 1 GHz (Pervushin et al. 1997). In this section, the optimal magnetic-field strength for the DIORITE analysis will be discussed.

The alignment induced TROSY shift change, $\Delta\delta_{TROSY}$, show significant magnetic-field dependency due to the RCSA contribution. The magnitude of RCSA is proportional to the applied magnetic-field strength, while the RDC is independent on the applied magnetic-field strength. The field dependency of the RCSA gives a peculiar profile to the $\Delta\delta_{TROSY}$ value.

In a peptide plane, the least shielded ^{15}N CSA tensor axis, δ_{xx}, is close to the NH bond; the angle β ranges from 15 to 20 degrees (Fig. 2b). The small β angle result in the cancellation between RDC and RCSA values to each other, making the observed $\Delta\delta_{TROSY}$ value smaller than the corresponding RDC. In most of the residues in a protein, RDC and RCSA have an opposite sign to each other. Therefore, $\Delta\delta_{TROSY}$ should be roughly equivalent to that a half of RDC minus RCSA in their absolute values. The value $\Delta\delta_{TROSY}$ tends to be approximately one-third of the RDC in an absolute magnitude.

The inter-cancellation effect depends on the magnetic-field strength, but the dependency is not linear. Using ubiquitin, we simulated the root mean square (rms) $\Delta\delta_{TROSY}$ values on different magnetic-field strengths indicated by the protein resonance frequencies. In the simulation, the rms $\Delta\delta_{TROSY}$, which should correspond to the average magnitude of $\Delta\delta_{TROSY}$, decreases up to 800 MHz and then increases according to the field strength. In lower magnetic-field strength, where the RCSA contribution is rather small and the $\Delta\delta_{TROSY}$ is roughly approximated by a half of RDC. The increasing RCSA, which has an opposite sign to RDC, contribution overall decreases the RDC value but further enhancement of the RCSA contribution in a higher magnetic field becomes dominant in $\Delta\delta_{TROSY}$ value, which may explain the profile.

The condition for weak alignment is carefully tuned to avoid severe signal broadening. The alignment order is typically tuned to around 10^{-3}, giving the maximal absolute magnitude of RDC around 20 Hz. Under the condition, $\Delta\delta_{TROSY}$ is expected to give about 6 Hz. Even under the worst 800 MHz, the expected $\Delta\delta_{TROSY}$ should be 5.5 Hz. The accuracy in reading peak positions at a signal-to-noise ration of 40:1 was estimated to be 0.6 Hz. Therefore, the experimental error in the observed $\Delta\delta_{TROSY}$ is estimated to be 0.8 Hz, in considering the error propagation through subtracting the TROSY shift in an aligned state by that in an isotropic state. Accordingly, the expected $\Delta\delta_{TROSY}$ is well resolved within the error in peak picking. It is noted that the estimated reading error in RDC should be 1.2 Hz due to twice subtraction required.

The resolution on TROSY spectrum is also the factor to be considered in discussing the performance of DIORITE on different magnetic-field strength. Using the average ^{15}N CSA tensor value estimated from ubiquitin, the dependencies of ^{15}N TROSY line width and rms $\Delta\delta_{TROSY}$ value are plotted against proton resonance frequencies, where the values are in ppb (parts per billion) units instead of Hz to compare them in the context of spectral resolution

(Fig. 12a). In this simulation, the optimal frequency to minimize the ^{15}N line width of the observed TROSY signal is 972.5 MHz, close but slightly different from the value by the simpler estimation in the original paper. In comparing the line narrowing of TROSY signal, the rms $\Delta\delta_{TROSY}$ value shows less dependency on the magnetic-field strength. The effective accuracy in observing $\Delta\delta_{TROSY}$ value should be estimated by the value $\Delta\delta_{TROSY}$ divided by the ^{15}N line width of TROSY signal (Fig. 12b). In this simulated profile, the optimal magnetic-field strength for observing $\Delta\delta_{TROSY}$ is around 900 MHz for ^{1}H resonance frequency. Therefore, the magnetic-field strength for the maximal TROSY effect is almost optimal for the DIORITE analysis. DIORITE analysis, thus, can take full advantage of the TROSY effect on a 900 MHz NMR spectrometer, which is now commercially available.

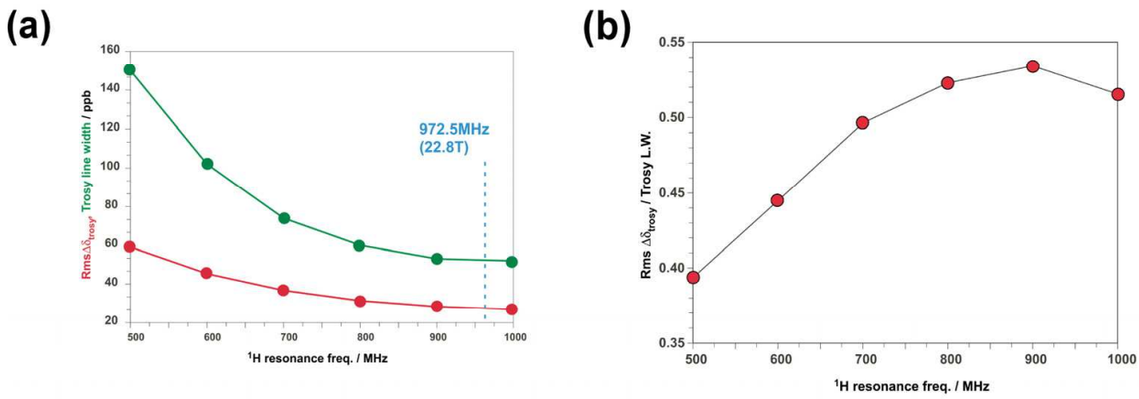

Fig. 12. Field dependency of the TROSY line width and the root-mean-square (rms) $\Delta\delta_{TROSY}$. (a) TROSY line width (green) and rms $\Delta\delta_{TROSY}$ (red) according to the magnetic field strength (b) Field strength dependency of the effective resolution in measuring $\Delta\delta_{TROSY}$.

5.4 Practical aspects of the DIORITE data collection

DIORITE analysis uses TROSY chemical shift changes $\Delta\delta_{TROSY}$ induced by a weak alignment of protein (Tate 2008, Tate et al. 2004). In general, chemical shift is very sensitive to the solution conditions, including temperature, sample concentration, pH, ionic strength and so no. In measuring $\Delta\delta_{TROSY}$, we have to exclude the other factors to change the chemical shift except for the alignment effects. To achieve this, anisotropically compressed polyacrylamide gel is the most appropriate medium for aligning protein. As described above, the anisotropically compressed gel (stretched gel) is made by inserting the cast gel chip having a little greater diameter than that of the inner diameter of NMR tube. The gel chip having the same diameter as that of NMR tube is not compressed after insertion, which can keep the isotropic cavity within. Protein in this non-compressed gel is not aligned and does not show any anisotropic spin interactions. The sample, therefore, can be used as the reference TROSY spectrum for measuring $\Delta\delta_{TROSY}$. Because the non-compressed gel consists of the same acrylamide composition, protein in this gel experiences the same chemical environments as in the compressed gel, which ensures that the observed TROSY shift changes solely come from the alignment effects. It is difficult in getting reference data with using the other

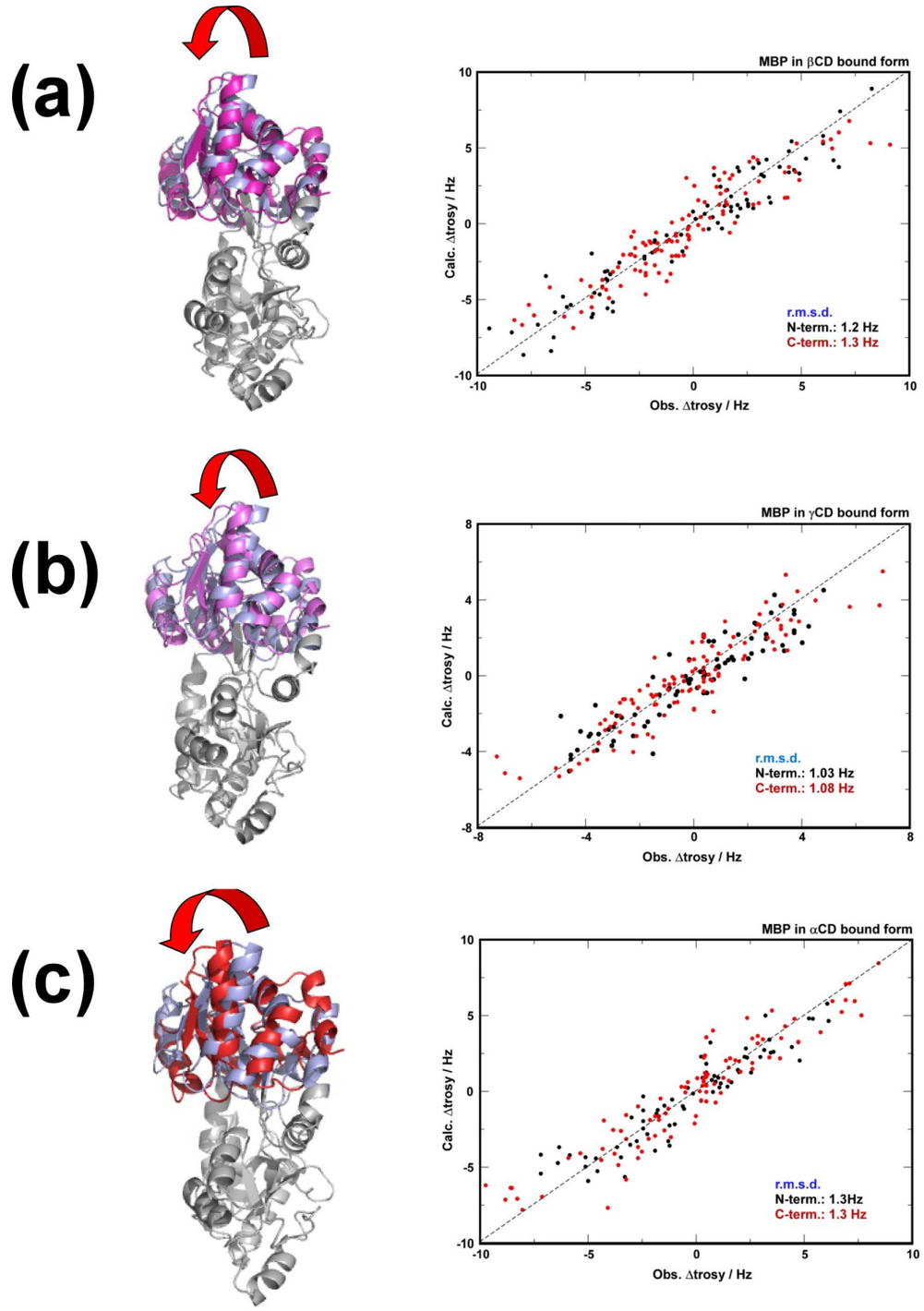

Fig. 13. Domain rotation angle change according to the ligand size in maltose binding protein (MBP). (a) β-CD, (b) γ-CD and (c) α-CD complex states. The hinge rotation angles induced by ligand binding were 13 deg., 14 deg. And 22 deg. for the cases of β-CD, γ-CD, and α-CD, respectively.

aligning media, including bicelle, filamentous phage. They cannot be the choice for DIORITE analysis.

In measuring $\Delta\delta_{TROSY}$ values, a set of TROSY spectra for the aligned and isotropic samples are used. The formation of the anisotropic cavity in the stretched gel can be monitored by the split of the deuteron signal from HOD; the deuteron in the water molecule within an anisotropic cavity shows a doublet, residual quadruplar coupling of the deuteron (Fig. 13a). The stronger anisotropy in a cavity gives a larger split. The water deuteron signal in the reference gel shows a singlet, confirming the cavity in the reference gel is isotropic.

In measuring NMR spectrum, water deuteron signal is used as a frequency lock to give the frequency standard. Because of the split of a deuteron signal in an aligned state, the resonance positions observed are biased; one of the doublet envelopes is used for the frequency lock, thus biasing the signals by a half of the split width. This offset should be subtracted from each signal position on the TROSY spectrum for protein in an aligned state.

5.5 DIORITE analyses on MBP in different ligand bound states

Here, we demonstrate the applications of the DIORITE analysis. Maltose binding protein (MBP) has two domains. From a series of X-ray analysis, MBP is known to show domain reorientation upon binding to ligand, and the domain rotation angle depend on size of the ligand molecule.

MBP binds to β-cyclodextrin (β-CD) comprising of seven glucose units, and it shows a slight change in the relative domain orientation from that in apo form as demonstrated by X-ray analysis. MBP also binds to different types of cyclodextrins comprising of the different number of glucose units; α–CD (six glucose units), γ-CD (eight glucose units). We expected to see the domain rotation angle changes according to the size of the three types of CDs.

Using the anisotropically compressed gel (stretched gel) and uncompressed reference gel, we collected a pair of TROSY spectra for each MBP in the complex with α-, β- and γ- CD. Using the apo-form MBP X-ray coordinate, we analyzed the relative domain orientation using DIORITE; the model structure was constructed based on the alignment tensors individually determined for N- and C-terminal domains. On each complex, the back-calculated and observed $\Delta\delta_{TROSY}$ values were well correlated, suggesting the alignment tensors for each domain were well determined (Fig. 13).

The DIORITE analyses on the MBP complexes demonstrated that for the smallest ligand, α-CD, the domain rotation angle was significantly larger than those for the β-CD complex structure. On the other hand, MBP in the complex with γ-CD retains almost the same domain orientation relative to the β-CD complex; the size over the β-CD does not change the domain rotation angle.

The example analyses demonstrated that the MBP showed significant domain reorientation according to the ligand size. It should be noted that the DIORITE analysis is very efficient to see this ligand-dependent domain reorientation; which requires just a pair of TROSY spectra collected for the sample in aligned and isotropic states.

6. Conclusion

X-ray structures are still exponentially accumulated every year. The huge collection of the protein coordinates should prompt the protein structure works using the existing protein

coordinate data. In this review, we introduced protein structure analysis in solution with the assistance of protein structure data collected by X-ray crystallography.

There has been a lot of discussion on the significance of the solution structure determination by NMR. Most of the structures for single domain proteins or isolated domains have shown marginal structural deviations from the corresponding structures solved by X-ray. This diminishes the importance of NMR structure analysis, except for the case in which crystallization is hard. When X-ray structure is available on a type of protein behaving as an independent structural unit, the solution structure determination on the protein by NMR is not usually conducted, because the crystal structure should not largely differ from that in solution. Additionally, in most of the cases, the size limitation in NMR structure determination prohibits such solution structure analyses, even if they are required. NMR solution structure analysis, therefore, has been recognized as a complementary method in rather limited cases.

The situation seems different in the structure analysis of multiple domain proteins. There already appeared some examples to show the difference in the domain orientations of protein between solution and crystalline states. The kinds of example will be increased, because it is getting to know that many proteins have domains linked by seemingly flexible or unstructured linkers judged from the sequence. In the proteins, it is presumable that the domain arrangement tends to be defined artificially by crystal packing, thus not represent the protein morphology in a solution state.

The NMR techniques using a weak alignment have paved ways to directly determine the relative domain orientation in solution, which has not been ever done by the conventional NMR methods. Some variations of the methods were introduced in this review, with their limitations in practical applications. Our devised DIORITE approach has a significant advantage in the domain orientation analysis over the existing methods, when it is applied to higher molecular weight proteins. The domain orientation analysis by DIORITE will expand the X-ray structure assisted reach in exploring the protein morphological change in solution, which associates with the functional exertion.

The domain rearrangement in protein, or protein morphological change, upon binding to ligand or interaction with its partner protein will become much more important in discussing protein functional regulation, after getting the high-resolution crystal structure in a specific state, for example, apo-form. The combined use of DIORITE with X-ray structure data may give vivid views how protein works in solution by changing its morphology. NMR is now becoming a complementary partner to X-ray crystallography in protein structure analysis, in particular, on higher molecular weight proteins.

7. Acknowledgement

S.T. acknowledges financial support from PRESTO/JST and SENTAN/JST. We appreciate RIKEN for accessing high-field NMR instruments. This review article is dedicated to Prof. Mamoru Tamura who demised on August 7th, 2011. He has been encouraging for progressing the work described here as a supervisor in the PRESTO/JST project.

8. References

Bax, A. (2003) Weak alignment offers new NMR opportunities to study protein structure and dynamics. *Protein Science,* 12, 1-16.

Berlin, K., D. P. O'Leary & D. Fushman (2009) Improvement and analysis of computational methods for prediction of residual dipolar couplings. *Journal of Magnetic Resonance,* 201, 25-33.

Bhattacharya, A., M. Revington & E. R. P. Zuiderweg (2010) Measurement and interpretation of 15N–1H residual dipolar couplings in larger proteins. *Journal of Magnetic Resonance,* 203, 11-28.

Boyd, J. & C. Redfield (1999) Characterization of 15N Chemical Shift Anisotropy from Orientation-Dependent Changes to 15N Chemical Shifts in Dilute Bicelle Solutions. *Journal of the American Chemical Society,* 121, 7441-7442.

Chou, J., S. Gaemers, B. Howder, J. Louis & A. Bax (2001) A simple apparatus for generating stretched polyacrylamide gels, yielding uniform alignment of proteins and detergent micelles*. *Journal of Biomolecular NMR,* 21, 377-382.

Clore, G. M. & C. D. Schwieters (2002) Theoretical and computational advances in biomolecular NMR spectroscopy. *Current opinion in structural biology,* 12, 146-153.

Conti, E., N. P. Franks & P. Brick (1996) Crystal structure of firefly luciferase throws light on a superfamily of adenylate-forming enzymes. *Structure,* 4, 287-98.

Cornilescu, G. & A. Bax (2000) Measurement of Proton, Nitrogen, and Carbonyl Chemical Shielding Anisotropies in a Protein Dissolved in a Dilute Liquid Crystalline Phase. *Journal of the American Chemical Society,* 122, 10143-10154.

de Vries, S. J., M. van Dijk & A. M. Bonvin (2010) The HADDOCK web server for data-driven biomolecular docking. *Nat Protoc,* 5, 883-97.

Dominguez, C., R. Boelens & A. M. Bonvin (2003) HADDOCK: a protein-protein docking approach based on biochemical or biophysical information. *J Am Chem Soc,* 125, 1731-7.

Evenas, J., V. Tugarinov, N. R. Skrynnikov, N. K. Goto, R. Muhandiram & L. E. Kay (2001) Ligand-induced structural changes to maltodextrin-binding protein as studied by solution NMR spectroscopy. *Journal of Molecular Biology,* 309, 961-974.

Fushman, D., N. Tjandra & D. Cowburn (1999) An Approach to Direct Determination of Protein Dynamics from 15N NMR Relaxation at Multiple Fields, Independent of Variable 15N Chemical Shift Anisotropy and Chemical Exchange Contributions. *Journal of the American Chemical Society,* 121, 8577-8582.

Goto, N. K., N. R. Skrynnikov, F. W. Dahlquist & L. E. Kay (2001) What is the average conformation of bacteriophage T4 lysozyme in solution? A domain orientation study using dipolar couplings measured by solution NMR. *Journal of Molecular Biology,* 308, 745-764.

Hajduk, P. J., G. Sheppard, D. G. Nettesheim, E. T. Olejniczak, S. B. Shuker, R. P. Meadows, D. H. Steinman, G. M. Carrera, P. A. Marcotte, J. Severin, K. Walter, H. Smith, E. Gubbins, R. Simmer, T. F. Holzman, D. W. Morgan, S. K. Davidsen, J. B. Summers & S. W. Fesik (1997) Discovery of Potent Nonpeptide Inhibitors of Stromelysin Using SAR by NMR. *Journal of the American Chemical Society,* 119, 5818-5827.

Hansen, M. R., L. Mueller & A. Pardi (1998) Tunable alignment of macromolecules by filamentous phage yields dipolar coupling interactions. *Nature structural biology,* 5, 1065-1074.

Hiyama, Y., C. H. Niu, J. V. Silverton, A. Bavoso & D. A. Torchia (1988) Determination of 15N chemical shift tensor via 15N-2H dipolar coupling in Boc-glycylglycyl[15N glycine]benzyl ester. *Journal of the American Chemical Society,* 110, 2378-2383.

Ishii, Y., M. A. Markus & R. Tycko (2001) Controlling residual dipolar couplings in high-resolution NMR of proteins by strain induced alignment in a gel. *Journal of Biomolecular NMR,* 21, 141-151.

Jain, N. U., S. Noble & J. H. Prestegard (2003) Structural characterization of a mannose-binding protein-trimannoside complex using residual dipolar couplings. *Journal of Molecular Biology,* 328, 451-462.

Kontaxis, G., G. M. Clore & A. Bax (2000) Evaluation of cross-correlation effects and measurement of one-bond couplings in proteins with short transverse relaxation times. *J Magn Reson,* 143, 184-96.

Kurita, J., H. Shimahara, N. Utsunomiya-Tate & S. Tate (2003) Measurement of 15N chemical shift anisotropy in a protein dissolved in a dilute liquid crystalline medium with the application of magic angle sample spinning. *J Magn Reson,* 163, 163-73.

Losonczi, J. A., M. Andrec, M. W. Fischer & J. H. Prestegard (1999) Order matrix analysis of residual dipolar couplings using singular value decomposition. *Journal of magnetic resonance (San Diego, Calif.: 1997),* 138, 334-342.

Loth, K., P. Pelupessy & G. Bodenhausen (2005) Chemical Shift Anisotropy Tensors of Carbonyl, Nitrogen, and Amide Proton Nuclei in Proteins through Cross-Correlated Relaxation in NMR Spectroscopy. *Journal of the American Chemical Society,* 127, 6062-6068.

Lundstrom, P., D. F. Hansen & L. E. Kay (2008) Measurement of carbonyl chemical shifts of excited protein states by relaxation dispersion NMR spectroscopy: comparison between uniformly and selectively (13)C labeled samples. *J Biomol NMR,* 42, 35-47.

Morris, G. M., R. Huey, W. Lindstrom, M. F. Sanner, R. K. Belew, D. S. Goodsell & A. J. Olson (2009) AutoDock4 and AutoDockTools4: Automated docking with selective receptor flexibility. *Journal of Computational Chemistry,* 30, 2785-2791.

Nakatsu, T., S. Ichiyama, J. Hiratake, A. Saldanha, N. Kobashi, K. Sakata & H. Kato (2006) Structural basis for the spectral difference in luciferase bioluminescence. *Nature,* 440, 372-376.

Ottiger, M. & A. Bax (1999) Bicelle-based liquid crystals for NMR-measurement of dipolar couplings at acidic and basic pH values. *J Biomol NMR,* 13, 187-91.

Ottiger, M., F. Delaglio & A. Bax (1998) Measurement of J and dipolar couplings from simplified two-dimensional NMR spectra. *J Magn Reson,* 131, 373-8.

Pervushin, K., R. Riek, G. Wider & K. Wuthrich (1997) Attenuated T2 relaxation by mutual cancellation of dipole-dipole coupling and chemical shift anisotropy indicates an avenue to NMR structures of very large biological macromolecules in solution. *Proc Natl Acad Sci U S A,* 94, 12366-71.

Prestegard, J. H., C. M. Bougault & A. I. Kishore (2004) Residual dipolar couplings in structure determination of biomolecules. *Chemical reviews,* 104, 3519-3540.

Sanchez, R. & A. Sali (2000) Comparative protein structure modeling. Introduction and practical examples with modeller. *Methods Mol Biol,* 143, 97-129.

Sass, J., F. Cordier, A. Hoffmann, M. Rogowski, A. Cousin, J. G. Omichinski, H. Lowen & S. Grzesiek (1999) Purple Membrane Induced Alignment of Biological Macromolecules in the Magnetic Field. *Journal of the American Chemical Society,* 121, 2047-2055.

Shuker, S. B., P. J. Hajduk, R. P. Meadows & S. W. Fesik (1996) Discovering High-Affinity Ligands for Proteins: SAR by NMR. *Science,* 274, 1531-1534.

Skrynnikov, N. R., N. K. Goto, D. Yang, W. Y. Choy, J. R. Tolman, G. A. Mueller & L. E. Kay (2000a) Orienting domains in proteins using dipolar couplings measured by liquid-

state NMR: differences in solution and crystal forms of maltodextrin binding protein loaded with beta-cyclodextrin. *J Mol Biol,* 295, 1265-73.

Skrynnikov, N. R., N. K. Goto, D. Yang, W. Y. Choy, J. R. Tolman, G. A. Mueller & L. E. Kay (2000b) Orienting domains in proteins using dipolar couplings measured by liquid-state NMR: differences in solution and crystal forms of maltodextrin binding protein loaded with beta-cyclodextrin. *Journal of Molecular Biology,* 295, 1265-1273.

Tate, S. (2008) Anisotropic nuclear spin interactions for the morphology analysis of proteins in solution by NMR spectroscopy. *Anal Sci,* 24, 39-50.

Tate, S., H. Shimahara & N. Utsunomiya-Tate (2004) Molecular-orientation analysis based on alignment-induced TROSY chemical shift changes. *Journal of magnetic resonance (San Diego, Calif.: 1997),* 171, 282-291.

Tjandra, N. & A. Bax (1997) Direct measurement of distances and angles in biomolecules by NMR in a dilute liquid crystalline medium. *Science,* 278, 1111-1114.

Tugarinov, V. & L. E. Kay (2003) Quantitative NMR studies of high molecular weight proteins: application to domain orientation and ligand binding in the 723 residue enzyme malate synthase G. *Journal of Molecular Biology,* 327, 1121-1133.

Tycko, R., F. J. Blanco & Y. Ishii (2000) Alignment of Biopolymers in Strained Gels: A New Way To Create Detectable Dipole−Dipole Couplings in High-Resolution Biomolecular NMR. *Journal of the American Chemical Society,* 122, 9340-9341.

Vijayan, V. & M. Zweckstetter (2005) Simultaneous measurement of protein one-bond residual dipolar couplings without increased resonance overlap. *Journal of Magnetic Resonance,* 174, 245-253.

Yao, L., A. Grishaev, G. Cornilescu & A. Bax (2010) Site-specific backbone amide (15)N chemical shift anisotropy tensors in a small protein from liquid crystal and cross-correlated relaxation measurements. *J Am Chem Soc,* 132, 4295-309.

Zweckstetter, M. (2008) NMR: prediction of molecular alignment from structure using the PALES software. *Nature Protocols,* 3, 679-690.

IntechOpen

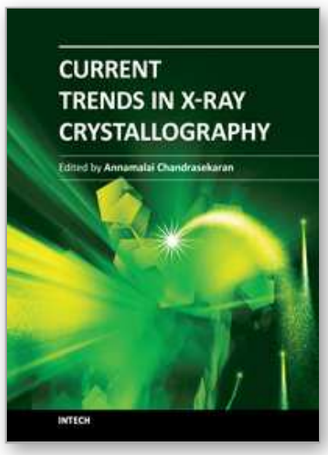

Current Trends in X-Ray Crystallography

Edited by Dr. Annamalai Chandrasekaran

ISBN 978-953-307-754-3
Hard cover, 436 pages
Publisher InTech
Published online 16, December, 2011
Published in print edition December, 2011

This book on X-ray Crystallography is a compilation of current trends in the use of X-ray crystallography and related structural determination methods in various fields. The methods covered here include single crystal small-molecule X-ray crystallography, macromolecular (protein) single crystal X-ray crystallography, and scattering and spectroscopic complimentary methods. The fields range from simple organic compounds, metal complexes to proteins, and also cover the meta-analyses of the database for weak interactions.

How to reference

In order to correctly reference this scholarly work, feel free to copy and paste the following:

Shin-ichi Tate, Aiko Imada and Noriaki Hiroguchi (2011). Complementary Use of NMR to X-Ray Crystallography for the Analysis of Protein Morphological Change in Solution, Current Trends in X-Ray Crystallography, Dr. Annamalai Chandrasekaran (Ed.), ISBN: 978-953-307-754-3, InTech, Available from: http://www.intechopen.com/books/current-trends-in-x-ray-crystallography/complementary-use-of-nmr-to-x-ray-crystallography-for-the-analysis-of-protein-morphological-change-i

INTECH
open science | open minds

InTech Europe
University Campus STeP Ri
Slavka Krautzeka 83/A
51000 Rijeka, Croatia
Phone: +385 (51) 770 447
Fax: +385 (51) 686 166
www.intechopen.com

InTech China
Unit 405, Office Block, Hotel Equatorial Shanghai
No.65, Yan An Road (West), Shanghai, 200040, China
中国上海市延安西路65号上海国际贵都大饭店办公楼405单元
Phone: +86-21-62489820
Fax: +86-21-62489821

© 2011 The Author(s). Licensee IntechOpen. This is an open access article distributed under the terms of the Creative Commons Attribution 3.0 License, which permits unrestricted use, distribution, and reproduction in any medium, provided the original work is properly cited.

IntechOpen

IntechOpen